**Title:** In-situ observation of FCC→HCP transformation-induced plasticity behavior during dynamic deformation of CoCrNi multi-principal element alloys

- J.A. Copley\*, Colorado School of Mines, Golden, CO 80401
- F.G. Coury, Universidade Federal de São Carlos, São Carlos, Brazil, 18052
- B. Ellyson, Colorado School of Mines, Golden, CO 80401
- J. Klemm-Toole, Colorado School of Mines, Golden, CO 80401
- J. Frishkoff, Colorado School of Mines, Golden, CO 80401
- C. Finfrock, Colorado School of Mines, Golden, CO 80401
- Z. Fisher, Colorado School of Mines, Golden, CO 80401
- N. Kedir, Purdue University, West Lafayette, IN 47907
- C. Kirk, Purdue University, West Lafayette, IN 47907
- W. Chen, Purdue University, West Lafayette, IN 47907
- N. Parab, Intel Co., Hillsboro, OR 97124
- T. Sun, University of Virginia, Charlottesville, VA 22904
- K. Fezzaa, Argonne National Laboratory, Lemont, IL 60439
- K.D. Clarke, Colorado School of Mines, Golden, Co 80401
- A.J. Clarke, Colorado School of Mines, Golden, CO 80401
- \*Corresponding author, email: amyclarke@mines.edu

#### Abstract

CoCrNi multi-principal element alloys (MPEAs) have potential as high toughness, blast resistant materials, but limited studies of their high strain rate behavior have been performed. Their high toughness has been attributed to low stacking fault energies and the activation of toughness enhancing deformation mechanisms, such as twinning- and transformation-induced plasticity (TWIP and TRIP, respectively), that may be affected by increased strain rate. This work examines a series of CoCrNi MPEAs tested with a miniaturized pressure bar, while simultaneous synchrotron x-ray diffraction and imaging are performed, and compares these results to those collected during quasi-static deformation at elevated temperatures. The collected diffraction indicates that TRIP was active at elevated strain rates for the most Co-rich alloys containing 50 or 55 at. pct. Co, while TRIP behavior was suppressed at elevated strain rates in a 40 at. pct. Co alloy anticipated to experience TRIP. The suppression of TRIP in the lower Co alloy at high strain rates is attributed to adiabatic heating, consistent with suppression of TRIP as a result of elevated temperatures.

# **Background and Introduction**

Multi-Principal Element Alloys (MPEAs) and related materials, such as High Entropy Alloys (HEAs), Medium Entropy Alloys (MEAs) and Complex Concentrated Alloys (CCAs), have grown in interest since their introduction in 2004 by Cantor and Yeh [1,2]. Some of these materials, including the equiatomic CoCrNi alloy, have shown promise as exceptionally damage tolerant materials, especially at cryogenic temperatures [3–5]. The discovery of CoCrNi's remarkable mechanical properties has resulted in a surge of interest in MPEAs that take advantage of specific deformation mechanisms, such as Twinning and Transformation Induced Plasticity (TWIP and TRIP, respectively), in search of more damage tolerant alloys [5–10]. TRIP and TWIP behaviors have been studied more extensively in advanced high strength steels, and are regarded as toughness enhancing deformation mechanisms, due to their ability to promote high work hardening rates and thus increased strength and uniform elongation [11–16]. While face-centered-cubic (FCC) CoCrNi remains the structural alloy with the highest reported fracture toughness, other works have produced evidence of non-equiatomic alloys with comparable or superior tensile strength and ductility [3,17]. Manganese containing MPEAs, such as those in the FeMnCoNi family, have also been shown to experience both TRIP and TWIP behaviors [18].

Recent work has shown that TRIP and TWIP effects may be enabled by alloying variations to the CoCrNi ternary, with Co- and Cr- rich alloys experiencing TRIP and Ni-rich alloys experiencing TWIP [19,20]. This is a result of Co's effect on stacking fault energy and the increased stability of the hexagonal-close-packed (HCP) phase [21-24]. Because TRIP behavior is produced by martensitic transformation from a parent to product phase (in this work, FCC→HCP), TRIP behavior is limited by the diffusionless transformation temperature. The diffusionless transformation temperature,  $T_0$ , is a thermodynamic factor describing the temperature at which two phases have the same free energy at a given composition. This serves as a limiting temperature for TRIP, because it is the temperature below which a free energy savings from the martensitic parent product phase transformation exists. As free energy savings from a transformation are generally larger far from  $T_0$ , for a given temperature below  $T_0$ , a high  $T_0$  may also indicate an increased driving force for TRIP behavior and thus a higher likelihood of TRIP as an operative deformation mechanism. Alloys in this work were deliberately selected to have a wide range of  $T_0$  values, in order to explore a range in behavior including both TRIP and TWIP phenomena.

Because CoCrNi and related alloys have excellent damage tolerance, even at cryogenic temperatures, it is anticipated they may exhibit promising properties at elevated strain rates and be suitable for performance in extreme environments <sup>[3,5,25]</sup>. This is supported by recent strain rate studies of FeMnCoCrNi and FeCoCrNi performed by *Shibani et al.*, as well as studies of FeCoCrNi performed by Zhang *et al.*, which show increased strength and ductility as a function of increasing strain rate <sup>[26,27]</sup>. While some dynamic testing has been performed on MPEAs, little work has been dedicated to examining the effects of strain rate on the activation of TRIP behavior, particularly in CoCrNi alloys, which is the aim of this work.

## **Experimental Methods**

Quasi-Static Testing of a Co<sub>55</sub>Cr<sub>40</sub>Ni<sub>5</sub> MPEA at Elevated Temperatures

A Co<sub>55</sub>Cr<sub>40</sub>Ni<sub>5</sub> (at. pct.) alloy (hereafter Co<sub>55</sub>) was predicted to experience TRIP using CALPHAD software. Specifically, Thermo-Calc software and the TCHEA3 database were used to identify alloys with high diffusionless transformation temperatures that lay within the single-phase region of the CoCrNi ternary phase diagram at 1200°C; this is a similar methodology to the work of Coury *et al* [19]. Co<sub>55</sub> was selected for its  $T_0$  of 967°C. While dual phase Fe-

- 61 containing MPEAs exist that exhibit good quasi-static mechanical properties, in CoCrNi the FCC
- region is bound by intermetallics, such as  $\sigma$ -phase, which can have deleterious effects on
- 63 mechanical properties  $^{[9,28]}$ . Figure 1 explores the range of  $T_0$  for CoCrNi alloys, so as to indicate
- TRIP potential of alloys with  $T_0$  above room temperature. A roughly 3 kg ingot of Co55 was
- produced via spray forming from commercially pure precursor material. Eight samples were also
- prepared by cold rolling, followed by heat treatment at 1200°C to recrystallize the material and
- ensure a fully FCC microstructure, before being machined by wire electro-discharge machining
- 68 (EDM). A schematic of the sample geometry is provided in the supplemental materials. Testing
- of the spray formed material was performed using a customized Gleeble 3S50<sup>TM</sup> thermo-
- 70 mechanical simulator at the XTMS beamline at the Brazilian Synchrotron Light Laboratory
- 71 (LNLS with a beam energy of 12KeV ( $\lambda = 0.1033 \dot{A}$ ) to perform simultaneous x-ray diffraction
- 72 (in reflection geometry off a 2x2 mm region of the sample) and quasi-static straining ( $\dot{\varepsilon} = 8.75 *$
- $10^{-4}s^{-1}$ ) at temperatures ranging from -100 to 900°C. Additional details regarding alloy
- selection and experimental methods are provided by Coury *et al.* [19,29].
  - High-Rate Testing of CoCrNi TRIP and TWIP MPEAs

- A series of five CoCrNi MPEAs were selected based on their ability to be heated into a
- single phase, FCC disordered solid solution and to have a range of diffusionless transformation
- 78 temperatures (in the method of Coury *et al.*) [19]. All thermodynamic data was generated using
- 79 ThermoCalc's TCHEA3 database, in which the CoCrNi ternary is fully assessed for all
- 80 compositions and temperatures. The selected alloys include four along the  $Co_X Cr_{40} Ni_{60-X}$  line,
- 81 with X = 30, 40, 50, and 55 (at. pct.), as well as the equiatomic  $Co_{33.33}Cr_{33.33}Ni_{33.33}$  alloy.
- These alloys are plotted onto a diffusionless transformation temperature map for the CoCrNi
- 83 ternary in **Figure 1**. Hereafter, these alloys are referred to only by their Co-content (e.g.,
- 84 Co<sub>40</sub>Cr<sub>40</sub>Ni<sub>20</sub> is Co<sub>40</sub>), aside from the equiatomic composition, which is referred to as CoCrNi.
- The diffusionless transformation temperatures for these alloys are presented in **Table 1**. This
- range of alloys was specifically selected for their range in diffusionless transformation
- 87 temperature such that they span a range of expected behaviors, with TRIP behavior expected in
- alloys with  $T_0 > 300 \, \text{K}$  and non-TRIP behavior in the alloys with  $T_0 < 300 \, \text{K}$ , allowing study
- 89 of how high-rate deformation affects the TRIP effect.

These alloys were prepared by arc-melting in an inert argon atmosphere from high purity components (99.9% or greater). The resulting buttons were then forged above 1000°C to improve their geometry for machinability. Twelve sub-sized, microscale tensile samples of each alloy were then machined using wire EDM and manually ground to final thickness of 100  $\mu$ m. A schematic of the sample geometry is provided in the supplemental materials. This thickness is required, due to the high attenuation coefficients of Co, Cr, and Ni for photons in the energy range used for synchrotron x-ray diffraction during deformation, as further described below. Finally, the samples were homogenized at 1150°C for 90 min before water quenching to room temperature to ensure a single-phase FCC microstructure. This heat treatment was verified by laboratory X-ray diffraction (Cu-K $\alpha$  radiation) to produce a single-phase FCC structure in all alloys, except for Co55, which shows some HCP to be present after quenching. As 1150°C is well above the FCC solvus for Co55, this is believed to be a result of martensitic transformation occurring prior to the testing during sample preparation and/or handling, rather than HCP that survived the heat treatment process.

The tensile samples were tested at Sector 32-ID-B at the Advanced Photon Source (APS) at Argonne National Laboratory with a modified tension bar (because of space limitations within the 32-ID-B hutch, only an incident bar, and not a transmitted bar, can be used) to perform high-rate tensile loading ( $\dot{\varepsilon} \approx 1000~s^{-1}$ ) with simultaneous synchrotron x-ray diffraction and imaging. Due to intensity requirements of the experiment, a quasi-single line beam from the U18 undulator at Sector 32-ID was used with an undulator gap of 12 mm, the intensity-energy spectra for this beam is shown in the supplemental materials. The first harmonic peak of this spectra is at 24.23 keV ( $\lambda = 0.5117~\dot{A}$ ). In an effort to sample as large a fraction of the sample as possible, the beam was focused to 1 x 2 mm<sup>2</sup>. More information on the high-rate loading instrument used may be found in Hudspeth *et al.* [30].

# **Results**

*Quasi-Static Testing of a Co<sub>55</sub>Cr<sub>40</sub>Ni<sub>5</sub> MPEA at Elevated Temperatures* 

Initial HCP in the spray-formed Co55 induced by machining was removed by a Gleeble heat treatment above 1200°C before quenching to the testing temperature, resulting in FCC microstructures prior to straining, without detectable HCP peaks in the XRD pattern shown in

**Figure 2**. During quasi-static straining at temperatures between -100 and 450°C, clear evidence of HCP peak evolution with strain is revealed, indicating the presence of deformation-induced martensitic transformation, or the TRIP effect. An example of the collected diffraction for the TRIP alloys is shown in **Figure 2**. At the highest temperature tested, 900°C, TRIP behavior was not observed, as indicated by the lack of peaks evolving with strain, see **Figure 3**. For the 600°C and 750°C cases, HCP peaks evolve as a function of strain, but continue to grow after failure has occurred in the sample. This can be rationalized by considering the greater extent of deformation occurring near the point of failure and the movement of the neck into the beam after the sample has failed.

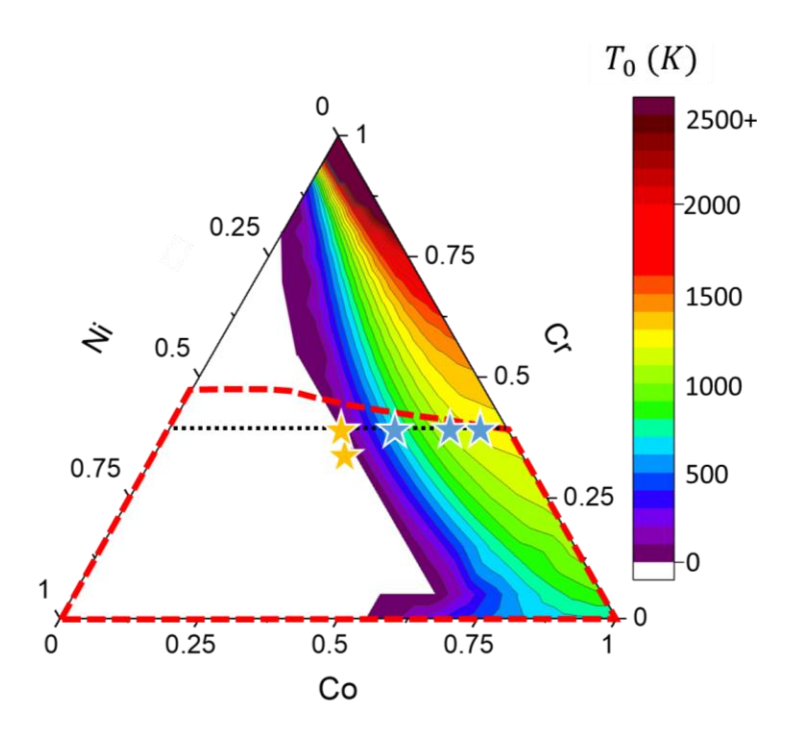


**Figure 1:** Diffusionless transformation temperatures ( $T_0$ ) of the CoCrNi ternary. Diffusionless transformation temperatures are increased by additions of Co and Cr, which stabilize the HCP phase. Ni acts to stabilize the FCC phase, with resulting Ni-rich alloys having low  $T_0$  to the point of the HCP phase never being lower in energy than the FCC phase, regardless of temperature ( $T_0 \le 0K$ ). The single phase FCC region at 1200°C is marked with a dashed red line. The  $Co_X Cr_{40} Ni_{60-X}$  line is marked by a black dotted line. Alloys believed to be TRIP enabled are marked by blue stars, and alloys believed to be TWIP enabled are marked by yellow stars.

**Table I:** Diffusionless transformation temperatures for the alloys tested. For cases where the relative stability of the FCC and HCP phases is such that there is no temperature at which the HCP is predicted to be more stable than the FCC,  $T_0$  is reported as D.N.E. or does not exist.

Alloy	<i>T</i> <sub>0</sub> (°C)
CoCrNi	D.N.E

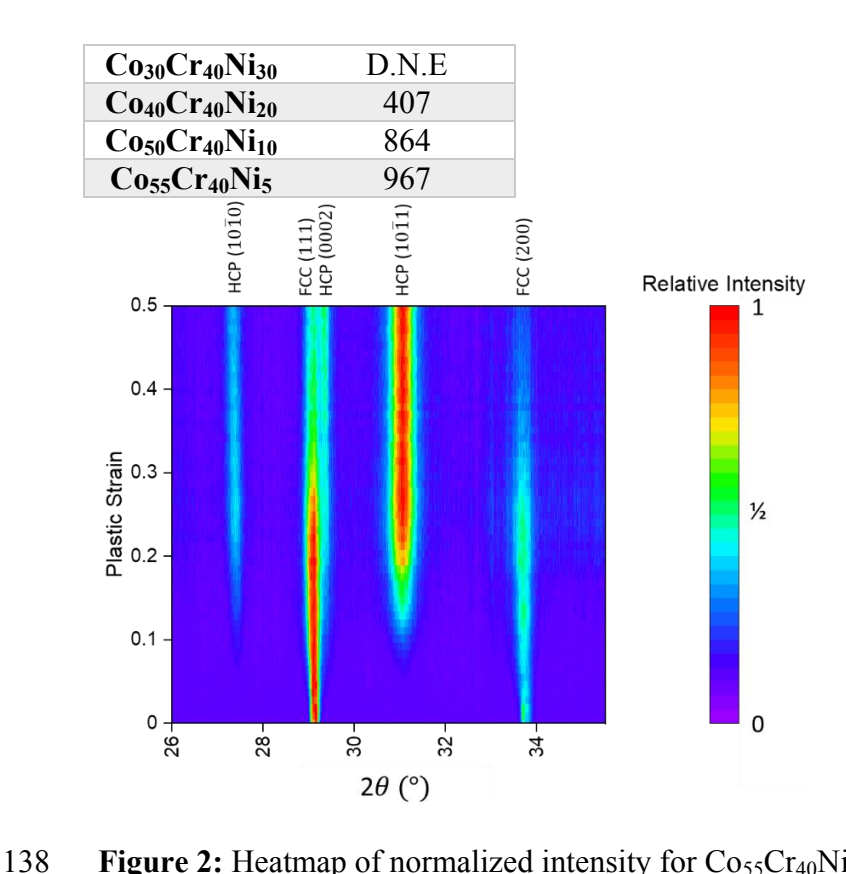


**Figure 2:** Heatmap of normalized intensity for  $Co_{55}Cr_{40}Ni_5$  tested at  $60^{\circ}C$ , showing the evolution of HCP peaks as a function of plastic strain from an initially pure FCC matrix. Detectable quantities of HCP begin forming at approximately 10% plastic strain, and the relative intensity of the HCP ( $10\overline{1}1$ ) peak continues to grow until approximately 20% plastic strain. The peaks are indexed and attributed to the FCC or HCP phases.

During the test, simultaneous crosshead motion in both directions was used to ensure the illuminated area of the sample was fixed, thus eliminating the effects of microstructural variation across the sample. However, after failure, the illuminated area of the sample changes in time due to continuing crosshead displacement. This would account for the near linear response of the HCP fraction with time after failure, as well as the close relation between the end of the crosshead displacement and time at which the plateau in HCP fraction is reached. This data is explored in the supplemental materials. It is not anticipated for the appearance of HCP peaks to be a result of a diffusional transformation, because similar behavior is not observed in the 900°C case, where the equilibrium microstructure is fully HCP and due to increased temperature, diffusion should proceed at a much more rapid rate. This indicates that TRIP is still occurring at 600°C and 750°C, but requires additional deformation to activate relative to the lower temperature cases.

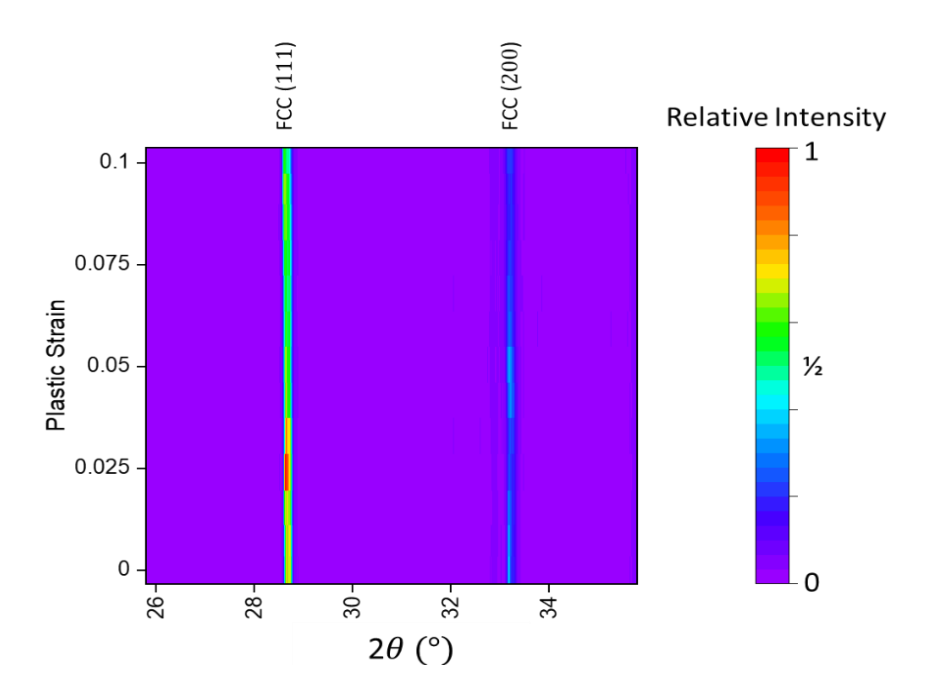


**Figure 3:** Heatmap of normalized intensity for  $Co_{55}Cr_{40}Ni_5$  tested at  $900^{\circ}C$ , showing no evolution of HCP peaks. This implies that either TRIP behavior was completely suppressed at this temperature, or so little transformation occurred prior to failure that it could not be detected by the diffraction. In either case, this indicates elevated temperatures, even when still below  $T_0$ , may result in suppressed TRIP behavior in CoCrNi alloys.

Because temperature correlates strongly with the activation of TRIP, analysis of the transformed fraction with plastic strain for all TRIP temperatures was performed. The relative intensity of the HCP phase was determined by analyzing the relative areas of the FCC (111) and HCP ( $10\overline{1}1$ ) peaks. Because the HCP (0002) peak overlaps with the FCC (111) peak, the area of the HCP ( $10\overline{1}0$ ) peak, scaled by its relative intensity relative to the HCP ( $10\overline{1}0$ ) peak, was subtracted from the area ascribed to the FCC (111) peak. Assessing these for the plastic strains of the different temperature tests, and then using a generalized logistic fit (**Equation 1**) to assess the growth of the HCP phase results in **Figure 4**. A difference in the behavior of the TRIP phenomenon as temperature increases is evident from both the plateaus and rates of transformation shown by the data. The generalized logistic curve used is defined by **Equation 1**, below:

$$(\varepsilon) = A + \frac{K - A}{(C + Q e^{-B\varepsilon})^{\frac{1}{\nu}}} \tag{1}$$

where A is the lower asymptote, K is the upper asymptote, Q is a factor relating to the initial HCP fraction prior to straining, B is the transformation rate, and V describes the asymmetry of the curve. The parameter C is generally taken as 1 and alters the upper asymptote from K when  $C \neq 1$ . To enable direct comparison of the upper plateaus from the fits, the value of C has been fixed at 1. Additionally, as the microstructures were all initially fully FCC, the value of C was assumed to be 0 for all cases. The details of the fits are found in **Table 2**. The LNLS diffraction data shows a decrease in both the rate of transformation (defined using the growth rate parameter, C is generalized logistic curve) and the extent of transformation (defined as the upper asymptote of the generalized logistic curve) with increasing testing temperature. These values, as well as the fraction of C and C and C for each temperature, are presented in **Table 2**.

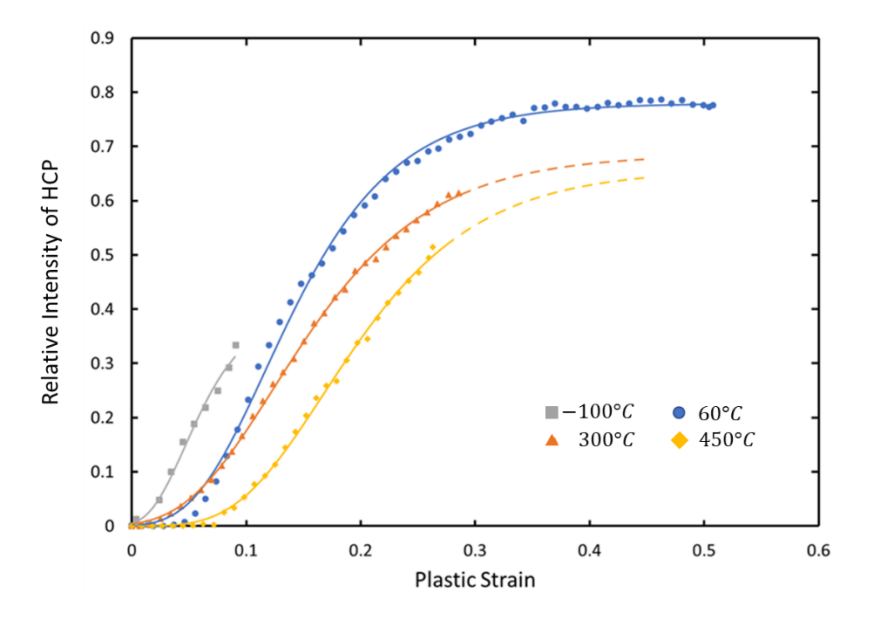


**Figure 4**: Plots of HCP fraction as a function of plastic strain for tests from -100 to 450°C, as determined from in-situ synchrotron x-ray diffraction experiments at LNLS, along with generalized logistic fits of the data to estimate the plateau heights of the samples that failed before the plateau was reached. This shows a decrease in the plateau height for the maximum HCP amount as a function of increasing temperature. Due to porosity inherent from the spray forming process, it is believed that samples other than that tested at 60°C failed prematurely as they had yet to reach a plateau in the FCC to HCP transformation, and as such were expected to have high work hardening rates that would prevent instability. The dashed lines associated with the 300 and 450°C tests are extrapolations of the plateau, given the logistic fit. The -100°C sample failed at too low a strain to estimate the plateau accurately. In addition to decreasing plateau height, the increasing temperatures resulted in decreased transformation amounts in the generalized logistic fits. In the plots, this appears as a decreasing slope of the near-linear portion of the logistic fits.

198

199

200

201

203

204

205

206

207

208 209

210 211

212

213

214

196 Of the alloys tested with simultaneous x-ray diffraction and imaging during high-rate 197 deformation with a tension bar, three of the five tested alloys (CoCrNi, Co30 and Co40) showed no experimental evidence of exhibiting TRIP type behavior, as no new peaks were evolved during the straining at 1000s<sup>-1</sup>. This does not necessarily mean that no HCP phase formed. In heavily deformed equiatomic CoCrNi, for example, nanometric layers of the HCP phase may form, which are difficult to detect using XRD [31]. The TRIP enabled Co50 showed evolution of a new peak attributable to HCP {1011}. The Co55, while containing initial HCP, showed 202 increased intensity of the HCP  $\{10\overline{1}1\}$  peak relative to the FCC  $\{111\}$  and  $\{200\}$  peaks. Examples of the collected diffraction patterns relative to the expected pattern for a complete FCC→HCP transformation in Co50, produced using the High Speed Polychromatic X-ray Diffraction (HiSPoD) software, are shown in **Figure 5** [32].

Table II: Parameters for fits of TRIP behavior as a function of temperature for Co<sub>55</sub>Cr<sub>40</sub>Ni<sub>5</sub>, showing decreasing upper asymptotes (K) as well as transformation rates (B) with increasing temperatures. Also shown are the relevant thermodynamic parameters to TRIP behavior,  $T_0$  and ΔG<sup>FCC→HCP</sup> for each temperature. 600°C and 750°C tests, which showed evolution of HCP after failure were not fit, as the HCP formation is better attributed to changes in the sampled region than deformation, and the 900°C test showed no HCP peak evolution.

Temperature	TRIP	K	В	$Q * 10^7$	$v * 10^7$	$T/T_0$	$\Delta G^{FCC \to HCP}$
(°C)							(J/mol)
-100	Y	0.399*	32.2	4.69	1.06	0.14	-2691.8
60	Y	0.779	15.9	4.64	0.73	0.27	-2288.1
300	Y	0.686	13.2	4.54	0.90	0.46	-1682.5
450	Y	0.657*	13.3	11.3	1.23	0.58	-1304.0
600	Y					0.70	-925.6
750	Y					0.83	-547.1
900	N					0.95	-168.6

<sup>\*</sup> Due to the limited strain at failure for the -100°C and 450°C, accurate prediction of the upper asymptote is not possible, resulting in a prediction just shortly above the HCP fraction at failure.

Due to the high ductility of CoCrNi alloys, a number of the samples did not fail in the initial straining wave, but rather failed in subsequent pulses. The mechanical data for the

subsequent loading was not collected. Examination of the mechanical response for the high-rate testing shows similar stress-strain response for all alloys other than Co55, which exhibits increased strength and reduced ductility. The sinusoidal shape of the example stress strain curves occurs due to ringing in the load cell from elastic wave propagation through the incident bar and sample. Representative stress-strain curves are shown in **Figure 6**.

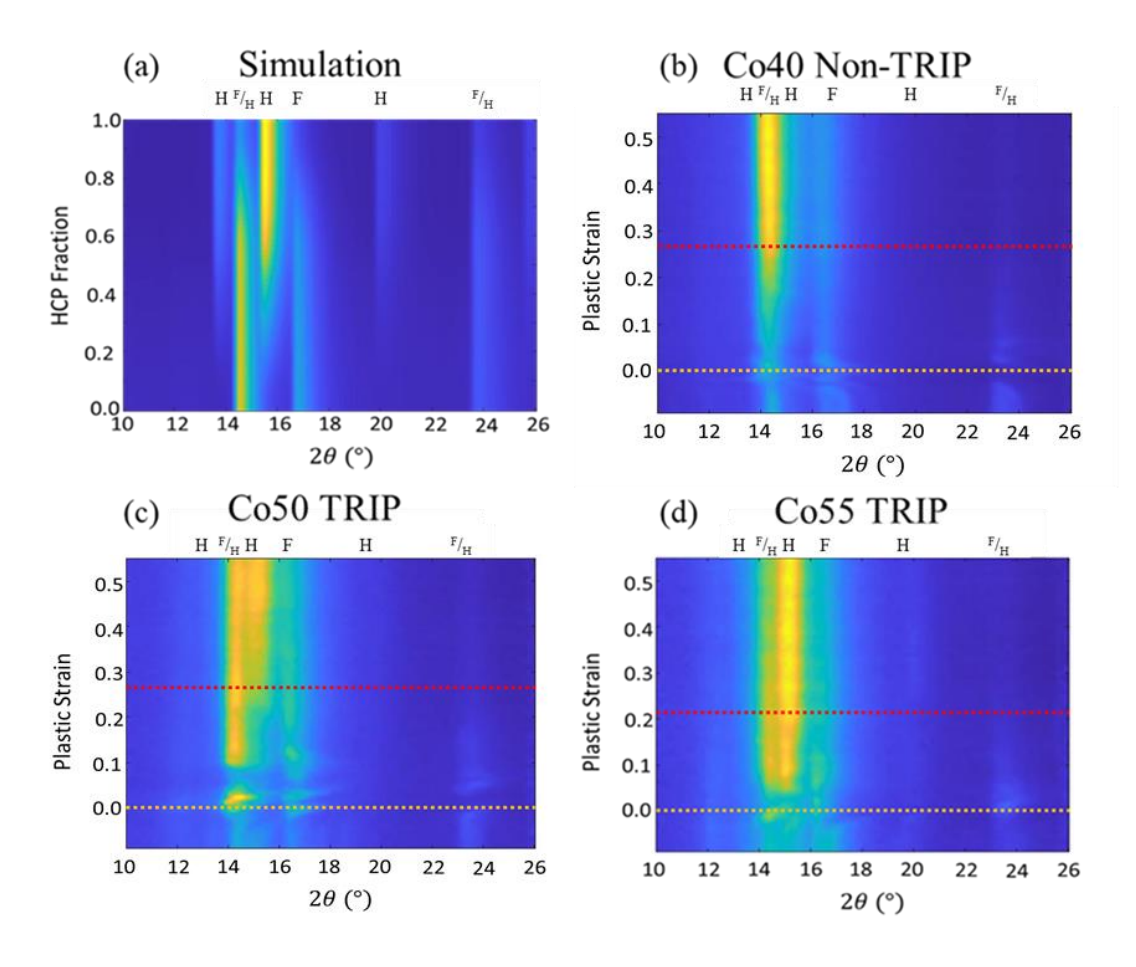


**Figure 5:** Comparison between (a) simulated diffraction patterns of different phase fractions of HCP and FCC for a Co50 alloy, showing a transformation from 100% FCC to 100% HCP, given the energy spectrum used for diffraction ( $E_{Peak} = 24.23 KeV$ ,  $\lambda_{Peak} = 0.5117 \dot{A}$ ) and a matching detector geometry to the experimental results. Experimental diffraction patterns of (b) Co40 (non-TRIP), (c) Co50 (TRIP), and (d) Co55 (TRIP) MPEAs. FCC and HCP peaks are marked with an F or H, respectively. Regions where FCC and HCP peaks overlap are marked as  $^{\rm F}$ /H. The onset of straining, as well as failure or the end of the first straining pulse, whichever occurred first, are marked with dotted lines (gold and red, respectively). Qualitative comparison between the simulated diffraction and collected patterns shows an HCP fraction of 40-60% in (c) the Co50 case at 30% strain, and of 60-80% in (d) the Co55 case at 20% strain. Results for other non-TRIP alloys (CoCrNi and Co30) are similar to (b) Co40. The increase in intensity of the Co40 peaks with strain is believed to be a result of increased transmission due to thinning during the tension test.

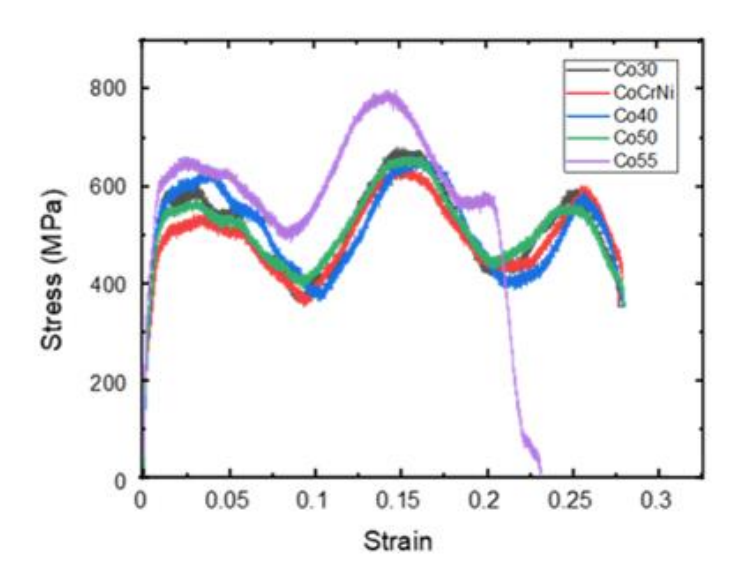


Figure 6: Mechanical response of alloys tested at  $1070 \pm 15s^{-1}$ . Co30, CoCrNi, Co40, and Co50 all demonstrate similar mechanical response to the high-rate deformation. Co55 showed limited ductility relative to the lower Co alloys. Only the Co55 alloy failed before the end of the first strain pulse.

#### **Discussion**

In the Co55 alloy tested at LNLS, suppression of TRIP behavior was seen even below  $T_0$ . Beginning at 600°C, TRIP initiation requires high strain levels relative to lower temperature tests, where TRIP was active even at low plastic strains (5% or less). In the 900°C test, no evidence of TRIP behavior was observed. The effect of temperature on the driving force for TRIP is clear. At high temperatures (approaching  $T/T_0=1$ ), the volumetric free energy savings for the martensitic transformation decrease. At  $T/T_0=1$ , there is no driving force for the transformation, and above this temperature, the forward progress of the reaction is energetically unfavorable. From the experiments at LNLS, it can be seen that the decrease in  $\Delta G^{FCC-HCP}$  results in decreasing HCP fraction with strain, as well as decreased rates of HCP formation with strain. This can be attributed to the decreasing driving force of the transformation. As the temperature increases, the TRIP phenomenon becomes less favorable. For the case of the Co55 at 600°C, as compared to 60°C, there is a decrease in driving force of over 1.3kJ/mol, or greater than one half of the driving force for TRIP at the lower temperature, as calculated via CALPHAD.

This reduction in driving force can also be examined as it relates to another property frequently correlated to an alloy's TRIP potential, the stacking fault energy. While for high SFE

materials deformation occurs mainly by dislocation slip, progressively lower SFE alloys may also have TRIP and TWIP mechanisms operating [33–35]. It is known that stacking fault energy,  $\gamma_{SFE}$ , increases with temperature. Therefore, TWIP would be favored at elevated temperatures compared to TRIP [36,37]. Using the Olsen-Cohen model of stacking fault energy in FCC materials and considering only the effect of changing  $\Delta G^{FCC \to HCP}$  for Co55 with temperature, it can be seen that stacking fault energy will increase by 82mJ/m<sup>2</sup> at 600°C relative to 60°C [38]. This suggests TWIP, or even only dislocation slip, occur at elevated temperatures. For comparison, measurement of  $\gamma_{SFE}$  for Co55 showed room temperature stacking fault energies in the range of 18-24  $mJ/m^2$ , which is consistent with the values reported for similarly Co-rich CoCrNi alloys by Koster *et al.* [39]. These data were generated using the method of Pierce *et al.* and are presented in **Figure 7** [40].

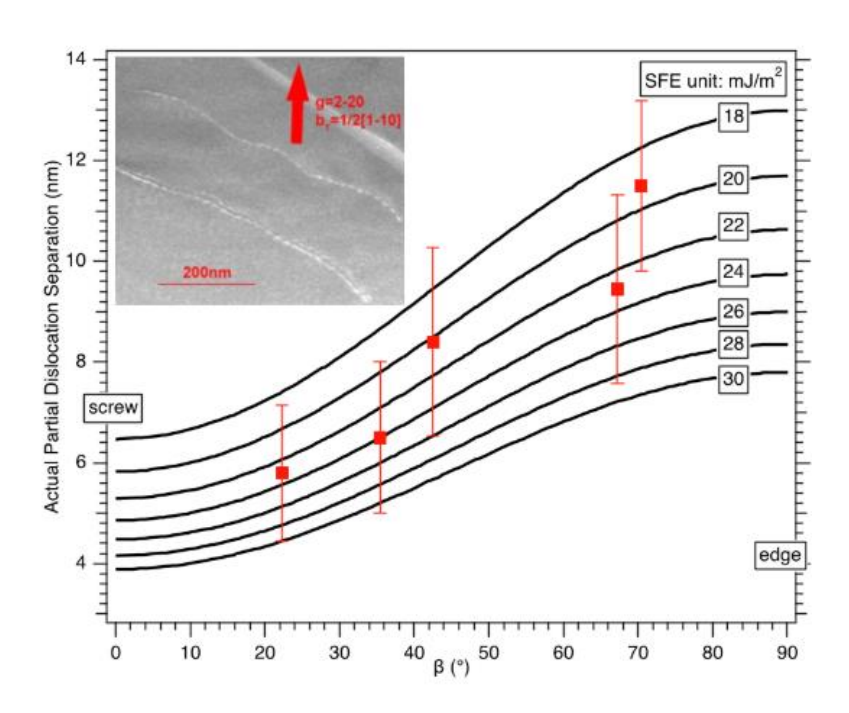


**Figure 7:** Measurements of stacking fault energy for Co55 at room temperature. These values are consistent with those reported in literature for Co-rich CoCrNi alloys, and are reflective of this alloy's potential to exhibit TRIP type behavior. Measurement of the stacking fault energy was performed by the method of Pierce *et al.* [40].

TRIP behavior was anticipated in the Co40, Co50, and Co55 alloys, both by consideration of thermodynamic factors like the diffusionless transformation temperature,  $T_0$ , and from previous work (for Co55). The Co40 alloy was expected to TRIP based on its  $T_0$  of

407°C and  $\Delta G^{FCC \to HCP}$  of -916 J/mol at room temperature, as well as TRIP behavior that has been observed in a similar alloy,  $\text{Co}_{36}\text{Cr}_{36}\text{Ni}_{28}$  [35]. As increased Ni acts to stabilize the FCC phase, it would be expected that increasing Ni at the expense of Co and Cr would result in an alloy less likely to TRIP, or conversely, that TRIP behavior would be promoted by decreasing Ni-content and replacing it with additional Co and Cr [41]. This suggests that the high strain rates employed acted to suppress TRIP.

Dynamic testing has several effects on sample response. In general, and analogously to low temperatures, high strain rates reduce the thermal contribution to dislocation motion and promotes deformation twinning [42,43]. Additionally, because the tests are short in duration, heat generated by plastic deformation during dynamic tests is unable to transfer to the surroundings and results in increased sample temperatures. Recent work by Soares et al. on an equiatomic FeMnCoCrNi alloy tested at strain rates up to 2800s<sup>-1</sup> has shown adiabatic heating can result in sample temperature increases of up to 80°C [44]. For the Co40, 80°C of adiabatic heating would result in a temperature of  $\approx 100$  °C, which is still below the diffusionless transformation temperature for Co40 of 407°C. At 380K (107°C), there is also a relatively large driving force for the FCC  $\rightarrow$  HCP transformation in Co40 ( $\Delta G_{378K}^{FCC \rightarrow HCP} = -724.6 J/mol$ ), allowing for the possibility of TRIP from a thermodynamic standpoint. However, volumes of HCP sufficient to be observed in the diffraction did not evolve. Due to high noise levels associated with diffraction during in-situ high strain rate testing, it is possible that HCP was evolved in low fractions or in nanometric layers, yielding undetectable signal in the Co40 diffraction patterns <sup>[25]</sup>. It is not clear from these experiments what minimum volume fraction of HCP would be required to produce observable diffraction peaks, but by referencing the simulated diffraction patterns in Figure 5, a conservative estimate would be 10-20%.

Comparing the driving force for the transformation in Co40 at 107°C to the driving forces of Co55 for the temperatures tested at LNLS shows that Co40 at 107°C has similar  $\Delta G^{FCC \to HCP}$  as Co55 between 600°C and 750°C, where TRIP behavior required greater strain to activate, and only low fractions of HCP were ever produced. This is also consistent with behavior in 304 stainless steel. Work by Hecker *et al.*, as well as other studies, has shown that increased strain rates and associated adiabatic heating result in significantly reduced TRIP behavior compared to quasi-static deformation, consistent with the lack of observed TRIP effect in the Co40<sup>[45–</sup>

<sup>48]</sup>.Although these studies are performed in a different alloy class, the thermodynamic and kinetic considerations for TRIP are similar and it is believed that qualitative comparisons of behavior between the alloy classes are valid.

It is believed that the alloys not exhibiting observable TRIP type behavior instead exhibited TWIP behavior, including the Co40 alloy. Considering high strain rate to be analogous to low temperatures, this behavior is consistent with the reported deformation mechanisms of Co-lean CoCrNi MPEAs  $^{[20,22,49]}$ . While TWIP is more difficult to observe by means of in-situ diffraction with only partial ring detectors, the collected area diffraction patterns, which initially contain only partial rings with discrete reflections, rapidly evolve into full rings during the initial straining. This behavior is consistent with deformation twinning, as twinned regions introduce new crystal orientations. Examples of initial partial rings and later full rings of a Co40 alloy are shown in **Figure 8**. While this is not solely indicative of TWIP behavior, in alloys like CoCrNi that have been extensively reported to experience significant deformation twinning, TWIP type behavior is the most probable explanation  $^{[20,22]}$ . The TWIP behavior of Co40 is also consistent with the behavior seen in this work of Co55 at elevated temperatures, where Co55 has similar  $\Delta G^{FCC \to HCP}$  and TRIP behavior is suppressed and replaced by another deformation mechanism.

Due to differences in processing (arc-melting vs. spray forming) and sample sizes, comparisons between the behaviors of the quasistatic and high-rate experiments are not perfectly straightforward. However, consideration of possible effects of these differences can be assessed to determine their significance when evaluating the rate effects on TRIP behavior in CoCrNi alloys. Grain size effects are important in TRIP behavior; however, they are not straightforward to assess. While finer grain sizes increase the total grain boundary area available as nucleation sites for the HCP phase, fine grains also tend to increase back-stresses and inhibit growth of the HCP phase [50–52]. Here, differences in the microstructure of the spray formed (initial grain size of spray formed Co55  $\approx 40 \mu m$ ) and are melted samples (initial grain sizes of are melted Co55  $\approx 33 \mu m$ ) may result in different strains being required for TRIP to activate. However, as the grain sizes are similar, this effect is expected to be small. More complicated is the effect of constraint on the deformation mechanism. Here, the thin samples are not expected to have a consistent through thickness strain state, however, the quasistatic tests were performed on thicker samples, but in a reflection geometry, and thus sampled the poorly constrained surface of the

thicker samples <sup>[53]</sup>. While the geometries are not identical, the similar lack of constraint in both samples suggests a likely similar response of the deformation mechanism. As the grain size and constraint influences are expected to be similar for the high-rate and quasistatic tests, observed differences are expected to be a result of the different strain rates. As TRIP behavior was suppressed during the high-rate experiments, it can be taken as an indicator that an effect of the high-rate deformation was responsible for the suppression of TRIP behavior in Co40.

332

333

334

335

336

337

338

339

340

341

342

343

344

345

346

347

348

349

350

351

352

353

354

355

356

357

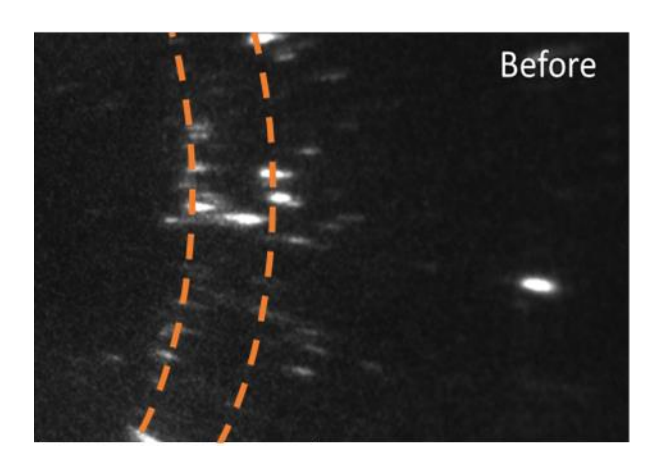
358

359

360

361

Exploration of the mechanical response of the high-rate data is complicated by ringing in the load cell and the fact that not all alloys failed consistently in the first pulse of strain. The data shows the Co55 alloy has higher strength, but lowered ductility compared to the other alloys tested (Figure 6). As tested, the Co55 was the only alloy with initial HCP phase in the microstructure. This initial HCP may result in the observed increase in strength and reduction in ductility compared to the other alloys. HCP present in the initial microstructure would result in increased yield strength as a result of a composite strengthening effect, in which HCP acts as a stronger phase compared to the FCC, as well as contributing to a dynamic Hall-Petch effect in which the martensite acts to reduce the effective grain size of the material. The reduction in ductility may also be attributed to the initial HCP, as the ductility in TRIP materials is a result of the high work hardening that the martensitic transformation promotes, which delays instability. By having initial HCP in the microstructure, the saturation of the transformation may occur at lower strains. As saturation of the transformation is expected to result in reducing work hardening rates, this may result in instability, and thus a reduction in ductility, although additional studies of the bulk mechanical response and associated microstructural characterization are warranted. It is possible that this initial HCP was formed as the result of unintentional straining of the thin samples. While this was not observed in the other alloys, which were handled similarly, the Co55 had the highest driving force for the FCC→HCP transformation. Accidental straining is difficult to avoid with the thin samples required for this kind of high-rate XRD, but as the load required to strain the material increases with part size, this is not expected to detract from performance in larger samples. While the ease of activating the FCC \rightarrow HCP transformation in these alloys makes them more challenging to study, we believe there are use cases, such as in high-rate impacts, that alloys with easily activated TRIP behavior are useful, and thus important to study.



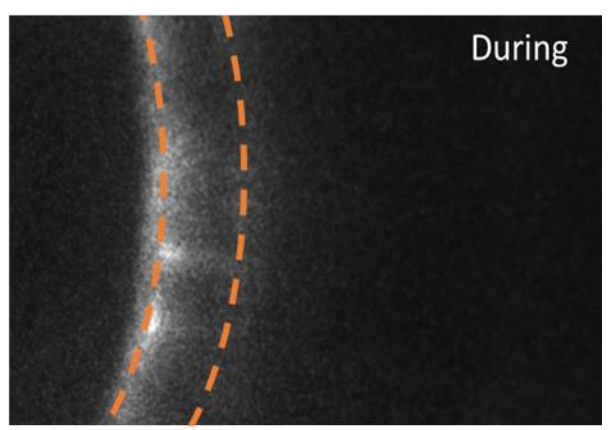


**Figure 8**: Evolution of full diffraction rings from initial partial rings with discrete reflections collected before and during straining of Co40 at high-rate (1000s<sup>-1</sup>) at the APS. This behavior is attributed to deformation twinning, which is promoted in FCC alloys during high-rate deformation, and has been shown to be a common deformation mechanism in the CoCrNi family of MPEAs. Expected positions of the FCC (111) and (200) diffraction rings are marked with dashed lines.

#### **Conclusions**

This work examined the suppression of TRIP behavior at temperatures below  $T_0$  during quasi-static straining of a Co-rich TRIP alloy. At elevated temperatures where  $\Delta G^{FCC \to HCP} \ge -1000 J/mol$ , TRIP was nearly completely suppressed, and at temperatures where  $\Delta G^{FCC \to HCP} \ge -200 J/mol$ , TRIP was suppressed completely. Assessing HCP evolution with plastic strain revealed that increasing temperature, and thereby decreasing the driving force for martensitic transformation, resulted in decreased extent of transformation. These results were compared to and used to explain the suppression of TRIP in a Co40 alloy during dynamic testing at  $1000s^{-1}$ . In this case, adiabatic heating and the low driving force for transformation act to suppress TRIP behavior and favor TWIP type behavior instead. Co-content was observed to dominate the activation of TRIP behavior, as it has a strong effect on the relative stability of the FCC and HCP phases and allowed for TRIP behavior to remain active for high Co alloys. TWIP remains active in CoCrNi at elevated strain rates, and becomes the primary deformation mechanism for Co40 when TRIP is suppressed.

Both TRIP and TWIP CoCrNi type alloys showed similar mechanical response at high strain rates, with the exception of the Co55 alloy, which had lower ductility and enhanced strength compared to the other alloys. This was attributed to the presence of martensitic HCP in the microstructure prior to straining. The initial HCP is believed to result in reduced ductility by

reducing the strain at which saturation of the FCC→HCP transformation occurs, resulting in reduced work hardening and the onset of instability. Additionally, the initial HCP phase in the Co55 is believed to result in increased strength of that alloy through a composite strengthening type effect. Additional work is needed to assess the relative mechanical properties of CoCrNi alloys deformed at high strain rates and explore the relationship between ductility and deformation mechanisms.

### Acknowledgements

386

387

388

389

390

391

392

413

414

393 This work was supported by the U.S. Department of the Navy, Office of Naval Research under 394 ONR award number N00014-18-1-2567. Any opinions, findings, and conclusions or 395 recommendations expressed in this material are those of the author(s) and do not necessarily 396 reflect the views of the Office of Naval Research. FGC, JKT, and KDC acknowledge support by 397 the Center for Advanced Non-Ferrous Structural Alloys (CANFSA), a National Science 398 Foundation Industry/University Cooperative Research Center (I/UCRC) [Award No. 1624836], 399 at the Colorado School of Mines (Mines). FGC also acknowledges CNPq, Conselho Nacional de 400 Desenvolvimento Científico e Tecnológico - Brasil (CNPq) [grant number 424645/2018-1]. This 401 research used resources of the Advanced Photon Source, a U.S. Department of Energy (DOE) 402 Office of Science User Facility operated for the DOE Office of Science by Argonne National 403 Laboratory under Contract No. DE-AC02-06CH11357; synchrotron x-ray data were collected at 404 the Sector 32-ID beamline. This research also used resources of the Brazilian Synchrotron Light 405 Laboratory (LNLS), an open national facility operated by the Brazilian Centre for Research in 406 Energy and Materials (CNPEM) for the Brazilian Ministry for Science, Technology, Innovations 407 and Communications (MCTIC). The XTMS beamline staff and Diego Santana, André Vidilli and 408 Lucas Otani are gratefully acknowledged for their assistance during the experiments. We also 409 gratefully acknowledge Dr. Yaofeng Guo stacking fault energy measurements and Gus Becker, 410 Christopher Finfrock, Yaofeng Guo, Chloe Johnson, Brian Milligan, Connor Rietema, Alec 411 Saville, and Doug Smith at Mines and Jinling Gao at Purdue University for their help performing 412 high strain rate testing at the APS.

#### **Conflict of Interest Statement**

On behalf of all authors, the corresponding author states that there is no conflict of interest.

## 415 References

- 416 1 B. Cantor, I.T.H. Chang, P. Knight, and A.J.B. Vincent: *Mater. Sci. Eng. A*, 2004, vol.
- 417 375–377, pp. 213–8.
- J.W. Yeh, S.K. Chen, S.J. Lin, J.Y. Gan, T.S. Chin, T.T. Shun, C.H. Tsau, and S.Y.
- 419 Chang: Adv. Eng. Mater., 2004, vol. 6, pp. 299–303.
- 420 3 B. Gludovatz, A. Hohenwarter, D. Catoor, E.H. Chang, E.P. George, and R.O. Ritchie:
- 421 *Science* (80-.)., 2014, vol. 345, pp. 1153–8.
- 422 4 Z.J. Zhang, M.M. Mao, J. Wang, B. Gludovatz, Z. Zhang, S.X. Mao, E.P. George, Q. Yu,
- 423 and R.O. Ritchie: *Nat. Commun.*, 2015, vol. 6, p. 10143.
- 424 5 B. Gludovatz, A. Hohenwarter, K.V.S. Thurston, H. Bei, Z. Wu, E.P. George, and R.O.
- 425 Ritchie: *Nat. Commun.*, 2016, vol. 7, pp. 1–8.
- 426 6 Y.H. Jo, W.M. Choi, D.G. Kim, A. Zargaran, S.S. Sohn, H.S. Kim, B.J. Lee, N.J. Kim,
- 427 and S. Lee: *Sci. Rep.*, 2019, vol. 9, p. 2948.
- 428 7 S.-H. Joo, H. Kato, M.J. Jang, J. Moon, C.W. Tsai, J.W. Yeh, and H.S. Kim: *Mater. Sci.*
- 429 Eng. A, 2017, vol. 689, pp. 122–33.
- 430 8 Y. Deng, C.C. Tasan, K.G. Pradeep, H. Springer, A. Kostka, and D. Raabe: *Acta Mater.*,
- 431 2015, vol. 94, pp. 124–33.
- 432 9 Z. Li, K.G. Pradeep, Y. Deng, D. Raabe, and C.C. Tasan: *Nature*, 2016, vol. 534, pp.
- 433 227–30.
- 434 10 Z. Li, F. Körmann, B. Grabowski, J. Neugebauer, and D. Raabe: *Acta Mater.*, 2017, vol.
- 435 136, pp. 262–70.
- 436 11 L. Liu, B. He, and M. Huang: *Adv. Eng. Mater.*, 2018, vol. 20, p. 1701083.
- 437 12 O. Bouaziz, H. Zurob, B. Chehab, J.D. Embury, S. Allain, and M. Huang: *Mater. Sci.*
- 438 *Technol.*, 2011, vol. 27, pp. 707–9.
- 439 13 S. Yan, T. Liang, Z. Wang, B. Yan, T. Li, and X. Liu: *Mater. Sci. Eng. A*, 2020, vol. 773,
- 440 p. 138732.

- 441 14 S.S. Sohn, H. Song, M.C. Jo, T. Song, H.S. Kim, and S. Lee: *Sci. Rep.*, 2017, vol. 7, p.
- 442 1255.
- 443 15 P.C. Maxwell, A. Goldberg, and J.C. Shyne: *Metall. Trans.*, 1974, vol. 5, pp. 1305–18.
- D.T. Pierce, J.A. Jiménez, J. Bentley, D. Raabe, and J.E. Wittig: *Acta Mater.*, 2015, vol.
- 445 100, pp. 178–90.
- 446 17 F.G. Coury, P. Wilson, K.D. Clarke, M.J. Kaufman, and A.J. Clarke: *Acta Mater.*, 2019,
- 447 vol. 167, pp. 1–11.
- 448 J. Tu, L. Liu, Y. Dou, C. Huang, L. Tan, L. Hu, Q. Sun, and Z. Zhou: *Mater. Sci. Eng. A*,
- 449 2018, vol. 737, pp. 9–17.
- 450 19 F.G. Coury, D. Santana, Y. Guo, J.A. Copley, L. Otani, S. Fonseca, G. Zepon, C.
- 451 Kiminami, M. Kaufman, and A. Clarke: Scr. Mater., 2019, vol. 173, pp. 70–4.
- 452 20 G. Laplanche, A. Kostka, C. Reinhart, J. Hunfeld, G. Eggeler, and E.P. George: Acta
- 453 *Mater.*, 2017, vol. 128, pp. 292–303.
- 454 21 W. Li, H. Fan, J. Tang, Q. Wang, X. Zhang, and J.A. El-Awady: Mater. Sci. Eng. A,
- 455 2019, vol. 763, p. 138143.
- 456 22 D.J. Siegel: *Appl. Phys. Lett.*, 2005, vol. 87, p. 121901.
- 457 23 M. Laurent-Brocq, A. Akhatova, L. Perrière, S. Chebini, X. Sauvage, E. Leroy, and Y.
- 458 Champion: *Acta Mater.*, 2015, vol. 88, pp. 355–65.
- 459 24 K. Sasaki, K. Yabuuchi, S. Nogami, and A. Hasegawa: J. Nucl. Mater., 2015, vol. 461,
- 460 pp. 357–64.
- 461 25 J. Miao, C.E. Slone, T.M. Smith, C. Niu, H. Bei, M. Ghazisaeidi, G.M. Pharr, and M.J.
- 462 Mills: *Acta Mater.*, 2017, vol. 132, pp. 35–48.
- 463 26 M. Shabani, J. Indeck, K. Hazeli, P.D. Jablonski, and G.J. Pataky: J. Mater. Eng.
- 464 *Perform.*, 2019, vol. 28, pp. 4348–56.
- 465 27 T.W. Zhang, S.G. Ma, D. Zhao, Y.C. Wu, Y. Zhang, Z.H. Wang, and J.W. Qiao: Int. J.
- 466 *Plast.*, 2020, vol. 124, pp. 226–46.

- 467 28 Z. Li, C.C. Tasan, K.G. Pradeep, and D. Raabe: *Acta Mater.*, 2017, vol. 131, pp. 323–35.
- 468 29 G. Faria, L. Wu, T. Alonso, A. Isaac, J. Piton, R. Neuenschwander, and A.J. Ramirez: in
- 469 In-situ Studies with Photons, Neutrons and Electrons Scattering II, Springer International
- 470 Publishing, 2014, pp. 245–59.
- 471 30 M. Hudspeth, B. Claus, S. Dubelman, J. Black, A. Mondal, N. Parab, C. Funnell, F. Hai,
- 472 M.L. Qi, K. Fezzaa, S.N. Luo, and W. Chen: in *Review of Scientific Instruments*, vol. 84,
- 473 American Institute of PhysicsAIP, 2013, p. 025102.
- 474 31 C.E. Slone, S. Chakraborty, J. Miao, E.P. George, M.J. Mills, and S.R. Niezgoda: Acta
- 475 *Mater.*, 2018, vol. 158, pp. 38–52.
- 476 32 T. Sun and K. Fezzaa: *J. Synchrotron Radiat.*, 2016, vol. 23, pp. 1046–53.
- 477 33 V. Borovikov, M.I. Mendelev, A.H. King, and R. LeSar: *Model. Simul. Mater. Sci. Eng.*,
- 478 2015, vol. 23, p. 055003.
- 479 34 R. Kalsar, P. Khandal, and S. Suwas: *Metall. Mater. Trans. A*, 2019, vol. 50, pp. 3683–
- 480 96.
- 481 35 Z. Yang, S. Lu, Y. Tian, Z. Gu, H. Mao, J. Sun, and L. Vitos: Designing Transformation-
- 482 Induced Plasticity and Twinning-Induced Plasticity Cr-Co-Ni Medium Entropy Alloys: Theory
- 483 and Experiment, Elsevier BV, 2020.
- 484 36 Y. Wang, B. Liu, K. Yan, M. Wang, S. Kabra, Y.-L. Chiu, D. Dye, P.D. Lee, Y. Liu, and
- 485 B. Cai: *Acta Mater.*, 2018, vol. 154, pp. 79–89.
- 486 37 S. Huang, W. Li, S. Lu, F. Tian, J. Shen, E. Holmström, and L. Vitos: Scr. Mater., 2015,
- 487 vol. 108, pp. 44–7.
- 488 38 G.B. Olson and M. Cohen: *Metall. Trans. A*, 1976, vol. 7A, pp. 1897–904.
- 489 39 E.H. Koster, A.R. Tholen, and A. Howie: *Philos. Mag.*, 1964, vol. 10, pp. 1093–5.
- 490 40 D.T. Pierce, J.A. Jiménez, J. Bentley, D. Raabe, C. Oskay, and J.E. Wittig: *Acta Mater.*,
- 491 2014, vol. 68, pp. 238–53.
- 492 41 G.N. Irving, J. Stringer, and D.P. Whittle: *Oxid. Met.*, 1974, vol. 8, pp. 393–407.

- 493 42 G.T. (Rusty) Gray: *Annu. Rev. Mater. Res.*, 2012, vol. 42, pp. 285–303.
- 494 43 Z.J. Jiang, J.Y. He, H.Y. Wang, H.S. Zhang, Z.P. Lu, and L.H. Dai: *Mater. Res. Lett.*,
- 495 2016, vol. 4, pp. 226–32.
- 496 44 G.C. Soares, M. Patnamsetty, P. Peura, and M. Hokka: J. Dyn. Behav. Mater., 2019, vol.
- 497 5, pp. 320–30.
- 498 45 K. Clarke: INFLUENCE OF STRAIN RATE ON THE MECHANICAL PROPERTIES
- 499 AND FORMABILITY OF FERRITIC STAINLESS STEELS, Colorado School of Mines. Arthur
- Lakes Library, 2002.
- 501 46 S.S. Hecker, M.G. Stout, K.P. Staudhammer, and J.L. Smith: *Metall. Trans. A*, 1982, vol.
- 502 13, pp. 619–26.
- J. Lichtenfeld and C.J. Van Tyne: 2004.
- 504 48 W.A. Poling: TENSILE DEFORMATION OF THIRD GENERATION ADVANCED HIGH
- 505 STRENGTH SHEET STEELS UNDER HIGH STRAIN RATES, Colorado School of Mines.
- 506 Arthur Lakes Library, 2016.
- 507 49 F.G. Coury, K.D. Clarke, C.S. Kiminami, M.J. Kaufman, and A.J. Clarke: Sci. Rep.,
- 508 2018, vol. 8, pp. 1–10.
- 509 50 J.R.C. Guimarães and P.R. Rios: *J. Mater. Sci.*, 2010, vol. 45, pp. 1074–7.
- 510 S. Takaki, H. Nakatsu, and Y. Tokunaga: *Mater. Trans. JIM*, 1993, vol. 34, pp. 489–95.
- 511 52 C.W. Sinclair, W.J. Poole, and Y. Bréchet: Scr. Mater., 2006, vol. 55, pp. 739–42.
- 512 53 M. Meyers and K. Chawla: *Mechanical Behaviors of Materials*, 2nd edn., Cambridge,
- 513 Cambridge, 2009.